EEET ECOLOGICAL ENGINEERING & ENVIRONMENTAL TECHNOLOGY

Ecological Engineering & Environmental Technology, 2026, 27(4), 343–354
https://doi.org/10.12912/27197050/219344
ISSN 2719–7050, License CC-BY 4.0

Received: 2026.02.19
Accepted: 2026.03.16
Published: 2026.04.01

Synergistic carbon dioxide mineralization in produced water for enhanced oil recovery: An experimental investigation

Mohannad Qassim M.A Aldayyeni [1], Usama Alameedy[1]

[1] Petroleum Department, College of Engineering, University of Baghdad, 10011 Baghdad, Iraq
* Corresponding author's e-mail: mohannad.ali2208@coeng.uobaghdad.edu.iq

ABSTRACT

This study investigates a synergistic approach to integrate carbon dioxide (CO_2) mineralization with hypersaline produced water (PW) from the Mishrif formation in Iraq's Al-Zubair oil field to generate "smart water" for enhanced oil recovery (EOR). The experimental methodology involved carbonating PW at 50 bar and 30 °C, followed by alkalinity adjustment to pH 10.4 using NaOH to induce mineral precipitation. A total precipitate yield of 8.78 g per 100 mL with significant CO_2 sequestration capacity of 7.5 g CO_2/L, was recovered. X-ray diffraction (XRD), scanning electron microscopy (SEM) and energy dispersive X-ray spectroscopy (EDS) analyses identified the crystalline mineral composition as calcite ($CaCO_3$, 19.95 wt%), fluorite (CaF_2, 16.63 wt%), and halite (NaCl, 9.07 wt%), with the remaining approximately 54% composed of amorphous phases and poorly crystalline materials. The transformation into "smart water" achieved a 24.7% reduction in interfacial tension (IFT), decreasing from 61.43 mN/m to 46.28 mN/m, primarily driven by pH-dependent interfacial charge effects. Also, zeta potential measurements showed a charge reversal from +12.4 mV to -19.08 mV, suggesting a favorable environment for altering reservoir wettability toward a more water-wet state. Inductively coupled plasma and optical emission spectrometry (ICP-OES) measurements initially indicated an increase in calcium concentration (from 9.663 to 12,847 mg/L) in a system undergoing precipitation determined to be caused by precipitate heterogeneity, dissolution during sample dilution and matrix effects inherent to hypersaline brines at extreme pH values. Absence of magnesium in XRD while there is a small amount in ICP-OES and EDS prove the recent studies on Mishrif formation in presence of dolomite.

Keywords: CO_2, produced water, mineralization, IFT, XRD, ICP-OES, SEM-EDS, Zeta Potential.

INTRODUCTION

Emissions of carbon dioxide (CO_2) are increasing at a rate of 2.4 ppm per year increased from 280 ppm in 1750 to 414.72 ppm in 2021, putting human life and ecosystems at risk. The combustion of fossil fuels is the primary source of greenhouse gases (GHGs), including CO_2, methane (CH_4), and nitrous oxide (N_2O) (Crippa et al., 2021)There are several types of emission scopes. "Greenhouse gas emissions are classified by scope: Scope 1 (direct emissions from fossil fuel combustion), Scope 2 (indirect emissions from electricity), and Scope 3 (supply chain and product-use emissions). Petroleum operations typically involve all three scopes. (Bello et al., 2023; Hansen et al., 2022; Vásquez et al., 2015). The Paris Agreement aims to limit the temperature rise to below 2 °C, preferably to 1.5 °C so global CO_2 emissions must be reduced to 45% by 2030 (Duval-Dachary et al., 2023). Carbon capture and storage (CCS) play an important role in climate change and recently the development of complex CO_2 capture and mineral sequestration materials has accelerated, and these technologies have been widely adopted in CCS, demonstrating significant potential (Liu et al., 2024). CCS depend on turning CO_2 into stable mineral carbonates that are safely stored in minerals. This is a long-term, safe, and effective way to store carbon and transforms and captured CO_2 into valuable minerals or products, providing sustainable feedstock for other industries (Lee et al., 2024; Matter et al., 2016). Carbon dioxide reacts with

calcium-containing materials (e.g., basalt, cement kiln dust) to produce calcium carbonate ($CaCO_3$) and with magnesium-rich minerals (e.g., peridotite, serpentine) to form magnesium carbonate ($MgCO_3$) (Guo et al., 2024; Huan et al., 2024; Huang et al., 2019; Liu et al., 2024).

This study demonstrates that the synergistic application of CO_2 and NaOH yields an interfacial tension (IFT) reduction of 24.7% at pH of 10.4 which indicates that a carbon-mineralization-based approach can achieve comparable performance to surfactant-enhanced methods even in low total acid number (TAN) environments, offering a dual benefit of improved recovery and carbon storage. Calcium-rich and high-salinity matrices require a strategic balance between minimizing matrix-induced interference and maintaining analytical sensitivity. High concentrations of chloride, sulfate, and easily ionized elements like sodium and calcium are known to cause significant signal suppression, ionization drift, and physical salt accumulation on instrument cones(Mahlknecht et al., 2004; Sakai and McCurdy, 2022; Søndergaard et al., 2015). While substantial dilutions sometimes exceeding 500-fold are often necessary to protect equipment and eliminate negative errors, which lead to inadequate detection limits for trace elements (Hein et al., 2017; Szymczycha-Madeja et al., 2021).In this study, ICP-OES samples were diluted with deionized water without acidification, which as discussed in Results presents potential for re-precipitation artifact. Standard protocols employing 2% HNO_3 acidification, so to mitigate these effects without compromising precision, researchers utilize internal standard corrections, such as Scandium, and rigorous matrix matching between samples and standards (Nadeau et al., 2018; Satya Chanakya and Misra, 2024). Recent studies have gaps in explored mineral sequestration in brine, such as (Alyousef et al., 2025) integrated mineralization with EOR by focusing on downhole brucite ($Mg(OH)_2$) precipitation but did not discuss IFT changes of the resulting mineralized brine. Similarly, while (Bennett et al., 2025) investigated calcium capture, but they encountered kinetic limitations with magnesium, and (Alshammari et al., 2025) focused on field-scale flow assurance rather than detailed interfacial property analysis. Also, the mineralization of brine using IFT and Zeta Potential for Mishrif produced water (PW) Al-Zubair oil field has not been previously investigated.

Produced water as a feedstock

The volume of produced water (PW) significantly outpaces oil production, yielding approximately 250 million barrels per day compared to 80 million barrels of oil in recent reports. The specific volume of PW is highly variable and depends on factors such as geographical location, reservoir history, and well age; in conventional fields, PW flow rates increase steadily over time which reaching up to 98% of the total extracted fluid in depleted reservoirs, whereas unconventional fractured wells typically exhibit a high initial flowback that gradually declines (Henderson et al., 1999; Li et al., 2006). To effectively repurpose this abundant byproduct for CO_2 mineralization, the PW must meet strict chemical criteria requires high concentrations of dissolved divalent cations (e.g., calcium and magnesium) to act as building blocks for precipitating solid, stable minerals like calcium carbonate ($CaCO_3$) and magnesium carbonate ($MgCO_3$). Because PW naturally lacks sufficient alkalinity for this reaction, its pH must be chemically elevated typically using an alkali like sodium hydroxide (NaOH) to an optimal range of 9 to 11, which ensures dissolved CO_2 is converted into the reactive carbonate ions (CO_3^{2-}) necessary for precipitation. Finally, the mineralization process must account for the complex composition of the brine; impurities such as chemical inhibitors can reduce CO_2 solubility, while heavy metals must be removed to prevent contamination of the final mineral product and ensure its safe, beneficial reuse.

CO_2 mineralization mechanisms

The most important processes include the dissolution of carbon dioxide and minerals, the reaction between carbonate ions and metal ions, and the precipitation of carbonate minerals. CO_2 in an aqueous solution first passes through the processes of hydration and dissociation, which results in the formation of carbonic acid. This acid subsequently breaks down into bicarbonate (HCO_3^-) and carbonate ions (CO_3^{2-}) with specific equations for the reaction processes in Equations:

CO_2 dissolution and hydration

$$CO_2(g) \rightleftharpoons CO_2(aq) \quad (1)$$

$$CO_2(aq) + H_2O(l) \rightleftharpoons H_2CO_3(aq) \quad (2)$$

Carbonite ions dissociation

$$H_2CO_3(aq) \rightleftharpoons HCO_3^-(aq) + H^+(aq) \quad (3)$$

$$HCO_3^-(aq) \rightleftharpoons CO_3^{2-}(aq) + H^+(aq) \quad (4)$$

Mineral carbonation reactions

$$Ca^{2+}(aq) + CO_3^{2-}(aq) \rightarrow CaCO_3(s) \quad (5)$$

Hydroxide precipitation:

$$Ca^{2+}(aq) + 2OH^-(aq) \rightarrow Ca(OH)_2(s) \quad (6)$$

Factors affecting CO_2 mineralization process

The efficiency of aqueous CO_2 mineralization is primarily governed by temperature, pH, and partial pressure. Because CO_2 solubility and reactivity drop significantly at elevated temperatures particularly above 200 °C lower temperatures, such as the 30 °C utilized in this study, are optimal for aqueous carbonation (Wiebe and Gaddy, 2002) Additionally, pH dictates the aqueous speciation of inorganic carbon: carbonic acid (H_2CO_3) dominates below pH 6.5, highly reactive bicarbonate (HCO_3^-) forms between pH 6.5 and 10, and carbonate ions (CO_3^{2-}) prevail above pH 10. Consequently, a pH range of 9–10 is considered optimal for maximizing both the thermodynamics and kinetics of carbonate precipitation (Mouedhen et al., 2017). Finally, in accordance with Henry's law, increasing the CO_2 partial pressure linearly enhances the concentration of dissolved CO_2 in the solution, which proportionally accelerates the carbonation reaction rates of minerals (Harrison et al., 2014; Werner et al., 2013).

Current technology landscape

Various CO_2 mineralization and capture techniques have been developed which presenting unique operational mechanisms and inherent limitations. Early *in-situ* applications involved injecting CO_2 into basaltic formations at elevated temperatures (50–150 °C) and pressures (368 psi), but these were heavily constrained by geological availability and the risk of wellbore clogging (Matter et al., 2011). Subsequent surface-level approaches introduced low-energy pH swing processes utilizing ion-exchange resins suffering from fouling and costly regeneration (Bustillos et al., 2024), as well as membrane-based gas/liquid diffusion systems that proved vulnerable to wetting and blocking in high-salinity brines (Xue et al., 2023). By 2025, focus shifted toward reactor-based and enhanced oil recovery (EOR) integrations. Continuous stirred-tank reactors (CSTR) successfully yielded 25% calcite production, though full mineral capture remained limited by slow magnesium kinetics (Bennett et al., 2025) and using Chitosan salt also used for sequestration CO_2 (Al-Yasiri-et al., 2025) . Integrating mineralization with EOR (using CO_2, NaOH, and brine) boosted oil Yasiri recovery by 22%, albeit offset by the high carbon debt of NaOH (Alyousef et al., 2025).Sequential precipitation field pilots using real brine at high pH (>10) have underscored ongoing flow assurance challenges, particularly the clogging of pumps and piping (Alshammari et al., 2025). New strategy for the potential use of common, and abundant but refractory feldspar for CO_2 sequestration was presented and tested. The novel mechanochemical processing of K-feldspar consisted of two-step high-energy ball milling(Achimovičová et al., 2025).

Study objectives

The primary objective of this research is to demonstrate a synergistic approach that integrates CO_2 mineralization with produced water to create "smart water" for Enhanced Oil Recovery (EOR):

- Demonstrate CO_2 mineralization of Mishrif PW and quantify the resulting precipitate composition.
- Quantify IFT and zeta potential changes across produced, carbonated, and smart water phases

MATERIALS AND METHODS

Materials

The sample of produced water which referred to (MQ: Mohannad Qassim, A: produced water) (MQA) used in CO_2 mineralization process has the salinity map as shown in Table 1.

Carbonated water, and smart water used in mineralization process referred to (MQB & MQC) which (MQ: Mohannad Qassim, B:carbonated water and C:smart water).The produced water from Mishrif formation in AL Zubair oil field in southern Iraq which the properties related to Mishrif Formation, dating to the Late Cenomanian–Early Turonian age, consists of a 100–200 m thick bioclastic-detrital limestone characterized by rudist bioherms and algal facies (Al-Ameri et al., 2009; Aqrawi et al., 1998; Mahdi and Aqrawi, 2014).

Table 1. Sample of produced water (MQA) from AL Zubair oil field

pH	Density	Ca^{2}	Mg	Na^{+}	SO_4	Cl^{-}	Others	TDS
5.9	1.19 gm/cm^3	9663 mg /L	6653 mg/L	34825 mg/L	665.95 mg/L	72746 mg/L	5447.05 mg/L	130000 mg/L

Located at a true vertical depth of 2.100–2.400 m, the reservoir exhibits estimated temperatures of 80–100 °C, initial pressures of approximately 3.200–3.500 psia, a total porosity of 15–28% (with an effective average of 20–22%), and high permeability ranging from 100 to 1.000 md (Lazim and Dawood, 2019; Rodrigues et al., 2016). The resident crude oil is classified as a medium gravity, sour, non-biodegraded oil with an API gravity of 23.3–28.9° (averaging 24.8°), an estimated viscosity of 2.0–5.0 cp, and high asphaltene and sulfur (4.2–5.36 wt.%) concentrations (Al Ibrahim et al., 2022; Awadh and Al-Mimar, 2023). Additionally, the aromatic-intermediate oil has a low total acid number (< 0.5 mg KOH/g) and an aromatic content exceeding 50%, having originated from Type II-S kerogen within Upper Jurassic Sulaiy and Lower Cretaceous Yamama marine carbonate source rocks that were deposited under anoxic, sulfate-reducing conditions.

Experimental setup and procedure

Figure 1 represents the process flow of CO_2 mineralization when the carbonated water was prepared by mixing 800 ml of produced water using a high-pressure, high-temperature (HPHT) mixing reactor of 1 liter in volume with CO_2 (purity 99%) operating at 500–600 RPM and 30 °C for 1 hour using different range of pressures (45, 50, 55, 60 and 65 bar)were tested to determine the optimum NaOH dose, which reaches pH ≥ 10. Pressures 45–65 bar were evaluated. Selection of 50 bar was based on: (1) achieving target pH 10.4 with economically reasonable NaOH consumption (6.1 g/100 mL vs. >8 g/100 mL at 65 bar) as in Figure 2, (2) literature precedent from (Bennett et al., 2025; Zhu et al., 2022) at similar pressures, and (3) equipment compatibility with standard pilot-scale HPHT systems. This multi-criteria optimization balances mineralization efficiency with practical field deployment considerations.

Mixing CO_2 with produced water on the surface leads to the formation of carbonic acid, which then reacts with dissolved Ca^{2+} ions. The addition of sodium hydroxide increases the pH, which facilitates the precipitation of minerals such as calcium carbonate ($CaCO_3$). pH values reported in Table 2.

The precipitation of Calcite ($CaCO_3$) is due to the reactions in previous Equations 5 and 6. For isolating the precipitated minerals in the resulting mixture, a 2–3 µm filter paper used. The precipitation dried in an oven at 50 °C for one day to ensure complete dryness.

Precipitate yield determination

The weight of Empty sample mass was 167.5 g before mineraliztion process. When the mineraliztion process finished the weight of the sample containing liquid and wet precipitate 280 g. Precipitate recovery was performed in triplicate,

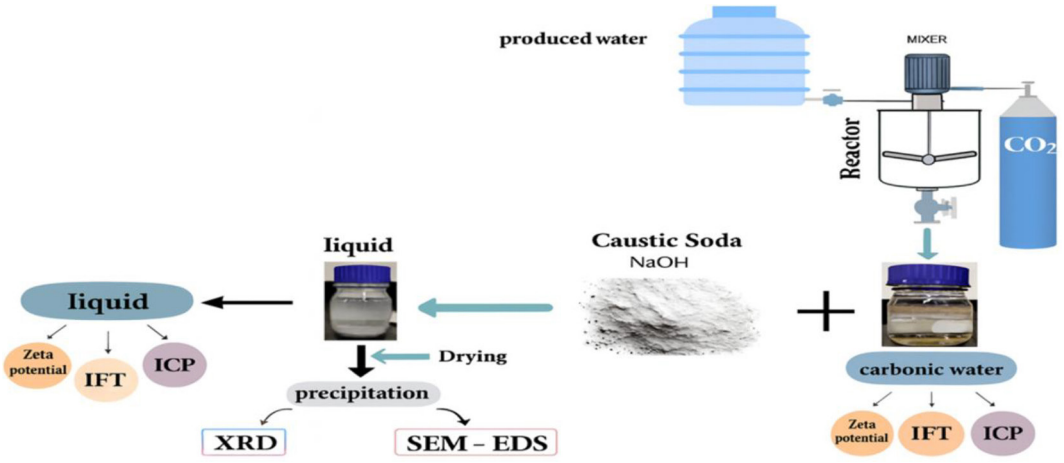

Figure 1. Process flow diagram for smart water generation via CO_2 mineralization of produced water

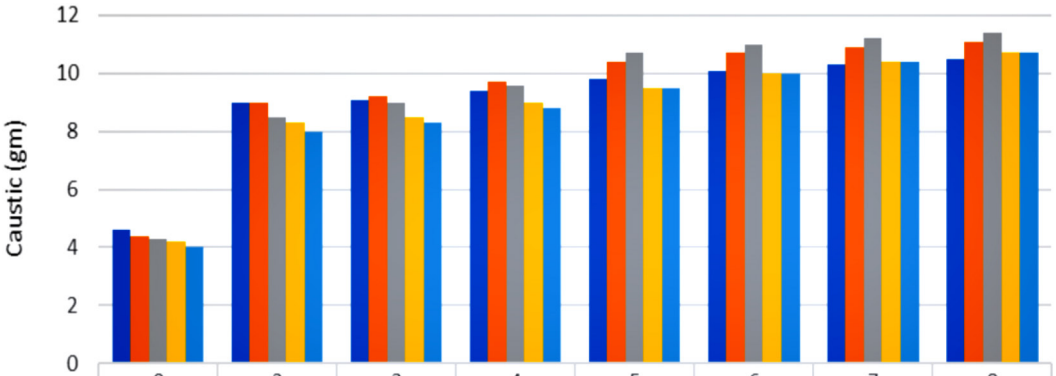

	0	2	3	4	5	6	7	8
45 bar	4.6	9	9.1	9.4	9.8	10.1	10.3	10.5
50 bar	4.4	9	9.2	9.7	10.4	10.7	10.9	11.1
55 bar	4.3	8.5	9	9.6	10.7	11	11.2	11.4
60 bar	4.2	8.3	8.5	9	9.5	10	10.4	10.7
65 bar	4	8	8.3	8.8	9.5	10	10.4	10.7

Figure 2. NaOH doses requirement to achieve alkaline pH at different CO_2 pressures

Table 2. pH values for 3 types of water

Sample no.	Description	pH
MQ A	Produced water	5.9
MQ B	Carbonic water	4.4
MQ C	Smart water	10.4

yielding 8.78 ± 0.05 g dry mass per 100 mL (mean ± standard deviation, n=3, relative standard deviation = 0.6%). Visual inspection revealed white crystalline powder with cubic (halite) and rhombohedral (calcite) crystal habits.

Subsequently, a series of analytical tests were conducted to characterize the precipitates. X-ray diffraction (XRD) to identify the crystalline structure and quantify mineral phases, scanning electron microscopy with energy dispersive X-ray spectroscopy (SEM-EDS) to examine surface morphology and perform elemental analysis and inductively coupled plasma optical emission spectroscopy (ICP-OES) to quantify dissolved cation concentrations in the three water types.

Analytical methods

Interfacial tension was measured using a KSV Sigma 703D Force Tensiometer via the Du Noüy ring method according to ASTM D971 standard. Zeta potential was measured by electrophoretic light scattering using a Brookhaven Zeta Plus analyzer. The measurements of participated materials – XRD patterns were collected using a Shimadzu XRD 6000 diffractometer with Cu Kα radiation according to ASTM E3294 standard. SEM-EDS analysis was performed using a TESCAN VEGA3 scanning electron microscope equipped with an Oxford Instruments energy dispersive X-ray detector. Elemental analysis was performed using a Horiba ICP-OES instrument.

RESULTS AND DISCUSSION

CO_2 mineralization efficiency

Experiments were conducted using a range of pressures from 45 to 65 bar at 30 °C. While 50 bar was selected as the optimal pressure to balance efficiency and cost. The NaOH consumption was 6.1 g/100 mL to reach the target pH. In contrast, increasing the pressure to 65 bar required significantly more NaOH (>8 g/100 mL), making it less economically viable. The raw produced water starts with a slightly acidic pH of 5.9.After mixing with CO_2 for one hour, the formation of carbonic acid drops the pH to 4.4. The final stage involves adding NaOH to reach a pH of 10.4 when carbonate ions (CO_3^{2-}) which become the dominant species when the pH exceeds 10 is necessary for mineral precipitation. The experimental procedure yielded 8.78 g of dry precipitate per 100 mL of produced water. The crystalline portion of this yield consists of calcite (19.95 wt%), fluorite (16.63 wt%), and halite (9.07 wt%).Amorphous phases which approximately 54% of the yield is

composed of amorphous or poor crystalline materials. The system achieved a CO_2 sequestration capacity of 7.5 g CO_2 per liter of produced water by converting dissolved CO_2 into stable mineral carbonates, effectively turning a waste product (produced water) into a carbon sink and a beneficial "smart water" for EOR.

Mineralogical characterization

The crystalline structure and mineralogical phases of the precipitates were characterized using X-ray diffraction, as shown in the diffractogram in Figure 3.

Phase identification and semi-quantitative quantification of the precipitates analyzed using X'Pert High Score Plus software (Malvern Panalytical). The analysis utilized the reference intensity ratio (RIR) method for extracting peak intensities from the full diffractogram (2θ 5–80°) and matching the mineral phases against the ICDD PDF-4 database. Based on the RIR calculations, the crystalline fraction of the sample consists predominantly of Calcite ($CaCO_3$, 19.95 wt%), Fluorite (CaF_2, 16.63 wt%), and evaporated Halite (NaCl, 9.07 wt%). Most of the sample (~54 wt%) was identified as amorphous or poorly crystalline material. Calcium carbonate hydrated mineral phases, and Mg-bearing hydroxides that contribute to the total mass (8.78 g) but fall below the RIR quantification threshold due to preferred orientation or lack of long-range order.

These crystallographic findings were detected by energy-dispersive X-ray spectroscopy (EDS) as shown in Figure 4. The EDS spectrum exhibited prominent calcium Kα and Kβ lines at 3.69 keV and 4.01 keV, which, coupled with strong low-energy peaks (<1 keV) for carbon and oxygen, strongly confirmed Calcite as a primary structural building block. Additionally, a distinct peak at 1.25 keV confirmed the presence of simple amount of magnesium, indicating the formation of brucite ($Mg(OH)_2$). The EDS scan also displayed visible peaks corresponding to sodium and chlorine from the Halite, alongside minor trace peaks for elements such as strontium (Sr), potassium (K), and niobium (Nb).

A comparative analysis of the elemental weight percentages derived from EDS and the crystalline phase quantification obtained via XRD provides a comprehensive validation of the precipitate's composition when The EDS results exhibit a dominant concentration of oxygen (44.78%), calcium (36.31%), and carbon (9.91%). Crucially, the observed carbon-to-calcium ratio in the EDS data serves as a near-perfect stoichiometric match for calcite ($CaCO_3$), strongly supporting the XRD findings to identifying calcite (19.95 wt%) as the primary crystalline carbonate phase. While XRD also quantified a significant fraction of fluorite (CaF_2, 16.63 wt%), Furthermore, the detection of sodium (1.88%) and chlorine (1.06%) by EDS directly showing that the XRD identification of evaporated halite (NaCl, 9.07 wt%) from the hypersaline brine. The slight discrepancy in the stoichiometric ratio of Na to Cl in the EDS data. EDS detected a substantial magnesium fraction (4.45%) that lacked a corresponding crystalline phase in the XRD profile. This disparity strongly suggests that the magnesium is either bound within an amorphous phase such as poor crystalline magnesium hydroxide or structurally incorporated into a mg-rich calcite lattice. Minor trace elements including potassium (K), strontium

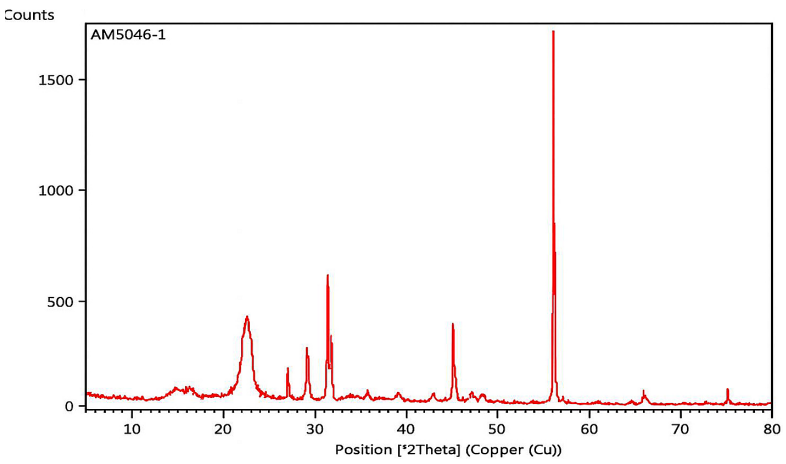

Figure 3. XRD analysis

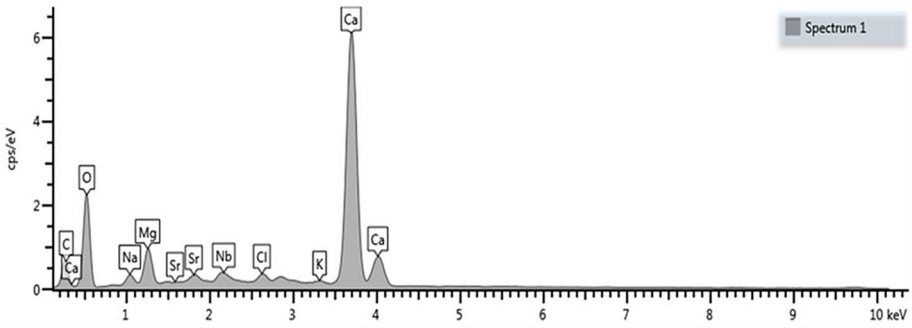

Figure 4. Compostion of precipitation materials

(Sr), and niobium (Nb) constituted 1.62% of the EDS weight, reflecting the natural trace impurities commonly trapped during rapid mineral precipitation from complex produced water brines.

EDS shows magnesium (4.45 wt%) while $Mg(OH)_2$ (brucite) is not resolved in XRD. This discrepancy suggests one of three possibilities: (1) magnesium precipitated as poorly crystalline or amorphous Brucite below the XRD detection limit, (2) magnesium exists as a trace dopant in calcite solid solution, or (3) magnesium remained dissolved and was not precipitated. Given the recent geological studies of the Mishrif Formation documenting dolomite in Wackestone microfacies (Al-Najm et al., 2025) as shown in Figure 5.

The surface morphology and structural integrity of synthesized materials are critical factors in determining their performance in applications such as catalysis and energy storage. To evaluate these characteristics, SEM was employed to visualize the particle distribution, size uniformity, and topographical features of the samples. The morphology at varying magnifications as shown in Figure 6, highlighting the transition from macro-scale grain distribution to individual particles geometry.

Mass balance and CO_2 sequestration capacity

- 100 mL of smart water sample (MQC) at the end of mineraliztion process yields 8.78 g.
- Halite (NaCl): 0.8 g (9.07%) → Evaporated brine salt, not CO_2 storage.
- Calcite ($CaCO_3$): 1.75 g (19.95%) → sequestered CO_2 (Equation 5).
- 1.75 g of calcium carbonate ($CaCO_3$) in sample 100 ml which $CaCO_3$ stoichiometry is $CaO{\cdot}CO_2$.
- Molecular weights: $CaCO_3$ = 100.09 g/mol, CO_2 = 44.01 g/mol.
- Moles of $CaCO_3$ = 1.75 g ÷ 100.09 g/mol = 0.017 mol.
- Moles of CO_2 sequestered = 0.017 mol (1:1 stoichiometry from Equation 5).
- Mass of CO_2 captured = 0.017 mol × 44.01 g/mol = 0.75 g CO_2 / 100 mL = 7.5 g CO_2 /L.
- Fluoride (CaF_2) which weights 0.16% (1.4 gm) is not contribute to CO_2 sequestration.

Figure 5. Wackestone microfacies in Zb-40 (2284.25 m) (Al-Najm et al., 2025)

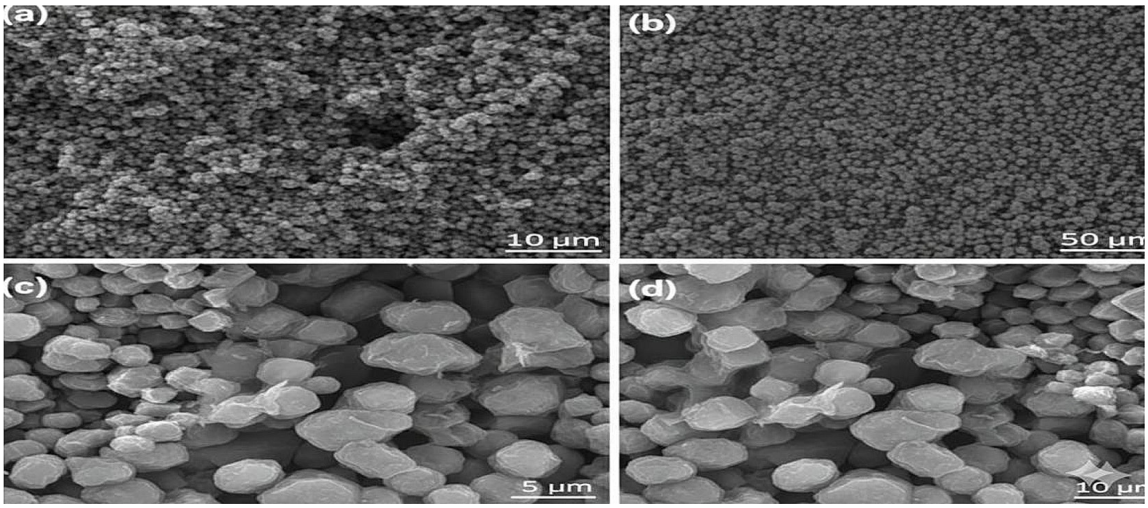

Figure 6. Scanning electron microscope (SEM) micrographs of various magnifications showing the surface morphology and particle distribution: (a, d) mid-range views (10 µm scale) showing a homogeneous distribution of monodisperse grains and inter-particle porosity, (b) low-magnification overview (50 µm scale) revealing a rugged, microporous bulk topography and dense particle aggregation, (c) high-magnification detail (5 µm scale)

The measured CO_2 sequestration capacity is 7.5 g CO_2/L, derived from the quantified Calcite precipitate (1.75 g $CaCO_3$ per 100 mL). The ratio of Fluorite (CaF_2, 1.4 g per 100 mL) represents additional calcium removal from solution but does not contribute to CO_2 sequestration. These results indicate that while 36 wt% of precipitate is calcium-based (combined $CaCO_3$ + CaF_2), approximately 20 wt% ($CaCO_3$) is associated with CO_2 mineralization process.

Interfacial properties and zeta potential

Interfacial properties for three types of water as shown in Table 3. Injecting CO_2 without alkalinity adjustment (MQ B) resulted in a minimal 7.2% reduction in interfacial tension (IFT) from the baseline, dropping to just 57.03 mN/m. Which indicates that acidic carbonated water alone provides limited interfacial modification (Nowrouzi et al., 2019). However, subsequent alkalinity adjustment to formulate the final Smart Water (MQ C) resulting 24.7% IFT reduction (to 46.28 mN/m). This significant improvement is driven by a charge reversal mechanism at the oil-water interface; at an elevated pH of 10.4, trace acidic functional groups (e.g., asphaltenes, resins, naphthenic acids) deprotonate which generating a negative interfacial charge. Additionally, a slight 4.2% increase in Na^+ concentration raises the ionic strength (from 2.2 to 2.244 M), compressing the electric double layer by 1% (0.20 to 0.19 nm) and creating ideal thermodynamic conditions for oil displacement.

Table 3. IFT values

Sample	IFT (mN/m)	Reduction
MQA (produced water)	61.43	–
MQB (carbonic water)	57.03	7.2 %
MQC (smart water)	46.28	24.7 %

Zeta potential measurements as in Figure 7 showed charge reversal from +12.4 mV (MQA/MQB) to −19.08 mV (MQC), indicating enhanced electrostatic repulsion between suspended precipitate particles and suggesting increased colloidal stability of the smart water phase. If these charged colloidal species were to adsorb or interact with rock surfaces during reservoir injection, they may contribute to wettability modification; however, direct validation through contact angle measurement or spontaneous imbibition studies would be required to establish wettability alteration.

Fluid chemistry and analytical observations

Fluid chemistry evaluated via Inductively coupled plasma optical emission spectrometry (ICP-OES) highlighted critical analytical challenges associated with hypersaline environments. Counterintuitively, the ICP-OES data showed an apparent increase in dissolved calcium from the baseline (MQ A: 9,663 mg/L) to

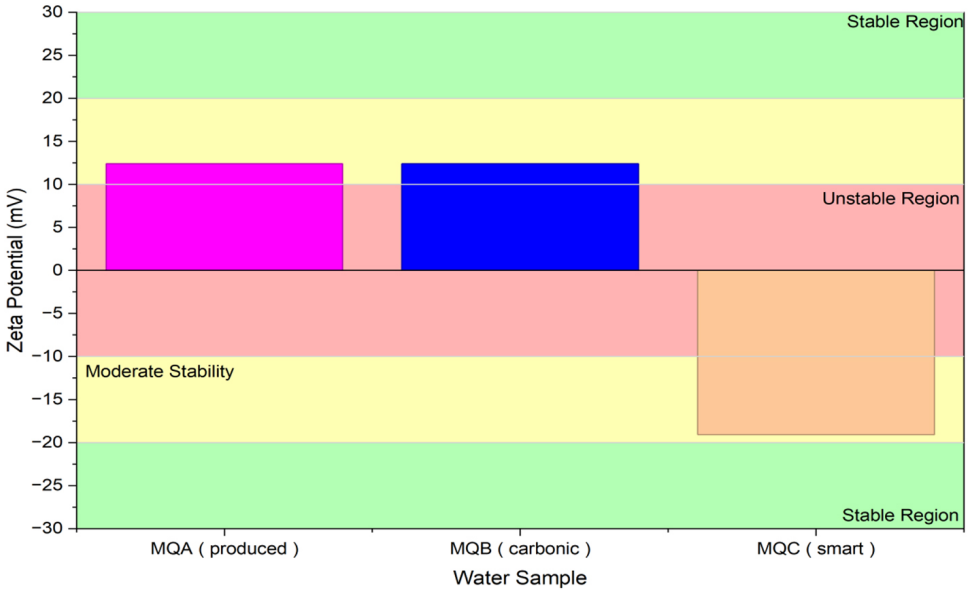

Figure 7. Zeta potential for 3 types of water

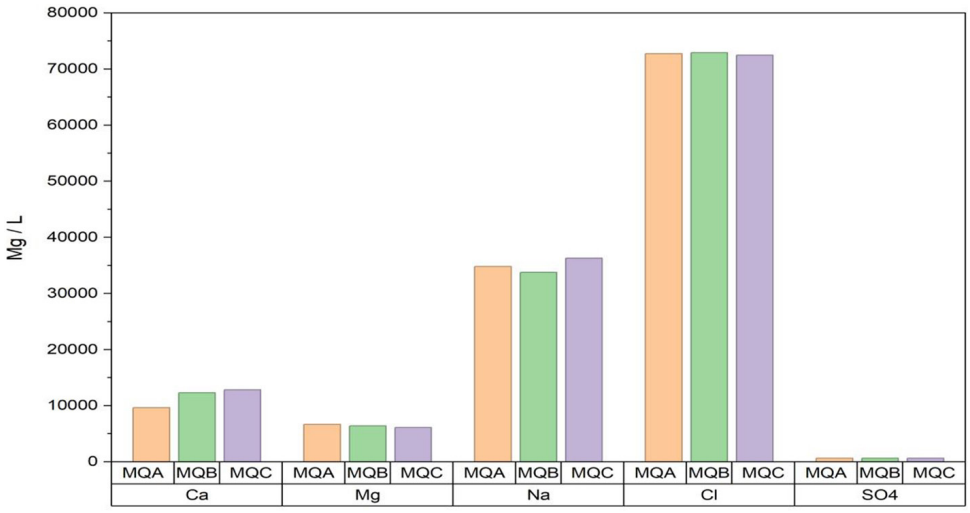

Figure 8. ICP-OES values

the carbonated (MQ B: 12,321 mg/L) and alkaline states (MQ C: 12,847 mg/L) as shown in Figure 8. This anomaly is attributed to strong matrix effects and high ionic strength inherent to the Mishrif produced water, which interferes with plasma atomization. Furthermore, the required dilution of the hypersaline samples prior to ICP-OES testing induced the re-dissolution of metastable amorphous precipitates back into the aqueous phase. Despite this apparent increase in dissolved Ca^{2+}, definitive solid-state characterizations (XRD and SEM-EDS) confirm that robust calcium carbonate precipitation occurred, proving that CO_2 was successfully mineralized despite the complex brine chemistry.

CONCLUSIONS

This study successfully demonstrated a synergistic approach for transforming hypersaline produced water into a “smart water” injection fluid while simultaneously achieving stable carbon sequestration.

The transformation of an alkaline “smart water” phase (pH 10.4) resulted in a 24.7% reduction in interfacial tension, decreasing from 61.43 mN/m to 46.28 mN/m. This reduction is primarily attributed to pH-dependent interfacial charge effects. Zeta potential measurements charge reversal from +12.4 mV in produced and carbonated water (MQA&B) to -19.08 mV in smart water(MQC) which reflects a favorable

electrochemical environment for altering reservoir wettability toward a more water-wet state, which is critical for maximizing resource recovery in carbonate reservoirs like Mishrif.

The measured CO_2 sequestration capacity is 7.5 g CO_2/L from the quantified Calcite precipitate (1.75 g $CaCO_3$ per 100 mL). The concurrent precipitation of Fluorite (CaF_2, 1.4 g per 100 mL) represents additional calcium removal from solution but does not contribute to CO_2 sequestration. Which indicate that while 36 wt% of precipitate is calcium-based (combined $CaCO_3$ + CaF_2), only ~20 wt% ($CaCO_3$) is associated with CO_2 mineralization under the tested conditions.

ICP-OES measurements initially indicated an increase in calcium concentration (from 9.663 to 12,847 mg/L) in a system undergoing precipitation. This anomaly was determined to be caused by several factors such as precipitate heterogeneity, dissolution during sample dilution (where metastable amorphous carbonates re-dissolve), and matrix effects inherent to hypersaline brines at extreme pH values.

REFERENCES

1. Achimovičová, M., Tóthová, E., Baláž, M., Zubrik, A., Briančin, J., Baláž, P., Erdemoglu, M., Birinci, M., Erdemoglu, S., Sis, H. (2025). In - situ capturing carbon dioxide capture by mechanochemical processing of K-feldspar with calcium oxide. *Journal of Ecological Engineering*, *26*(5), 401–409. https://doi.org/10.12911/22998993/200661
2. Al Ibrahim, R. N., Al-Owaidi, M. R. A., Alnajen, F. M., Al-Khafaji, A. J. (2022). Investigation of the geochemical properties and origin of the crude oils accumulated in the Mishrif Reservoirs in the Zubair, Halfaya, and Buzurgan Oilfields, Southern Iraq. *The Iraqi Geological Journal*, 98–110. https://doi.org/10.46717/igj.55.2B.9Ms-2022-08-25
3. Al-Ameri, T. K., Al-Khafaji, A. J., Zumberge, J. (2009). Petroleum system analysis of the Mishrif reservoir in the Ratawi, Zubair, North and South Rumaila oil fields, southern Iraq. *GeoArabia*, *14*(4), 91–108. https://doi.org/10.2113/geoarabia140491
4. Al-Najm, F. M., Al-Samer, H. A., Shehab, M. N., Mahdi, M. M. (2025). Integrating reservoir properties with microfacies analysis of the Mishrif formation at Zubair Oilfield, Iraq. *Iraqi Journal of Science*, *66*(8), 3267–3283. https://doi.org/10.24996/ijs.2025.66.8.18
5. Alshammari, S., Saleem, H., Cha, D., Ayirala, S. (2025, September 16). CO_2 mineralization in produced water: Transforming waste brines into a carbon sink. *Middle East Oil, Gas and Geosciences Show (MEOS GEO)*. https://doi.org/10.2118/227029-MS
6. Al-Yasiri, A. K., Alameedy, U., Al Mukainah, H., Abdulhamid, M. A., Al-Yaseri, A. (2025). Chitosan salt as a dual-function agent for CO_2 sequestration and acidizing enhancement. *Journal of Molecular Liquids*, *437*. https://doi.org/10.1016/j.molliq.2025.128324
7. Alyousef, M. H., Alshammari, S., Al-Yaseri, A. (2025). Synergy of CO_2 mineralization in produced water with enhanced oil recovery: An experimental study. *Fuel*, *382*, 133694. https://doi.org/10.1016/j.fuel.2024.133694
8. Aqrawi, A. A. M., Thehni, G. A., Sherwani, G. H., Kareem, B. M. A. (1998). Mid-cretaceous Rudist-bearing carbonates of the Mishrif formation: an important reservoir sequence in the Mesopotamian basin, Iraq. *Journal of Petroleum Geology*, *21*(1), 57–82. https://doi.org/10.1111/j.1747-5457.1998.tb00646.x
9. Awadh, S. M., Al-Mimar, H. S. (2023). The effect of nickel, vanadium, asphaltene, NSO and sulfur on crude oil quality. *The Iraqi Geological Journal*, 137–144. https://doi.org/10.46717/igj.56.2B.10ms-2023-8-19
10. Bello, A., Ivanova, A., Cheremisin, A. (2023). A comprehensive review of the role of CO_2 foam EOR in the reduction of carbon footprint in the petroleum industry. *Energies*, *16*(2), 1167. https://doi.org/10.3390/en16031167
11. Bennett, Q., Wolfe, K. D., Kasick, A., Shaffer, R., Nyamekye, E., Movil-Cabrera, O., Thackery, M., Oza, S., Trembly, J. (2025). Semi-continuous ex situ carbon dioxide mineralization in produced water for calcite production. *Energy Science & Engineering*, *13*(7), 3678–3687. https://doi.org/10.1002/ese3.70125
12. Bustillos, S., Christofides, M., McDevitt, B., Blondes, M., McAleer, R., Jubb, A. M., Wang, B., Sant, G., Simonetti, D. (2024). Ion exchange processes for CO_2 mineralization using industrial waste streams: pilot plant demonstration and life cycle assessment. *Chemistry Select*, *9*(18). https://doi.org/10.1002/slct.202400834
13. Crippa, M., Solazzo, E., Guizzardi, D., Monforti-Ferrario, F., Tubiello, F. N., Leip, A. (2021). Food systems are responsible for a third of global anthropogenic GHG emissions. *Nature Food*, *2*(3), 198–209. https://doi.org/10.1038/s43016-021-00225-9
14. Duval-Dachary, S., Beauchet, S., Lorne, D., Salou, T., Helias, A., Pastor, A. (2023). Life cycle assessment of bioenergy with carbon capture and storage systems: Critical review of life cycle inventories. *Renewable and Sustainable Energy Reviews*, *183*, 113415. https://doi.org/10.1016/j.rser.2023.113415

15. Guo, L., Peng, X., Wang, Q., Zhao, Y., Xu, L., Wu, S. (2024). Research progress on carbon dioxide mineralization sequestration technology by tailings. *Green and Smart Mining Engineering*, *1*(3), 307–321. https://doi.org/10.1016/j.gsme.2024.08.005
16. Hansen, A. D., Kuramochi, T., Wicke, B. (2022). The status of corporate greenhouse gas emissions reporting in the food sector: An evaluation of food and beverage manufacturers. *Journal of Cleaner Production*, *361*, 132279. https://doi.org/10.1016/j.jclepro.2022.132279
17. Harrison, A. L., Power, I. M., Dipple, G. M. (2014). Accelerated carbonation of brucite in mine tailings for carbon sequestration. *Environmental Science & Technology*, *48*(9), 126–134. https://doi.org/10.1021/es3012854
18. Hein, C., Sander, J. M., Kautenburger, R. (2017). New approach of a transient ICP-MS measurement method for samples with high salinity. *Talanta*, *164*, 477–482. https://doi.org/10.1016/j.talanta.2016.06.059
19. Henderson, S. B., Grigson, S. J. W., Johnson, P., Roddie, B. D. (1999). Potential impact of production chemicals on the toxicity of produced water discharges from north sea oil platforms. *Marine Pollution Bulletin*, *38*(12), 1141–1151. https://doi.org/10.1016/S0025-326X(99)00144-7
20. Huan, Q., Wibowo, H., Yan, M., Song, M. (2024). A review of CO_2 mineral storage: Current processes, typical applications, and life cycle assessment. *Journal of Environmental Chemical Engineering*, *12*(6), 114785. https://doi.org/10.1016/j.jece.2024.114785
21. Huang, H., Guo, R., Wang, T., Hu, X., Garcia, S., Fang, M., Luo, Z., Maroto-Valer, M. M. (2019). Carbonation curing for wollastonite-Portland cementitious materials: CO_2 sequestration potential and feasibility assessment. *Journal of Cleaner Production*, *211*, 830–841. https://doi.org/10.1016/j.jclepro.2018.11.215
22. Lazim, A.. A., Dawood, H. S. (2019). Structural geology and petrophysics analysis to Injection wells of Mishrif Formation in Shuaiba Dome – Zubair oil field. *Journal of Petroleum Research and Studies*, *9*(3), 59–74. https://doi.org/10.52716/jprs.v9i3.314
23. Lee, S., Kim, E., Lee, D., Jang, K., Park, J., Choi, W. Y. (2024). Synthesis of seawater-derived superhydrophobic calcium carbonate via CO_2 mineralization by utilizing L-Arginine/L-Lysine oleate-based self-assembly structures. *Chemical Engineering Journal*, *490*, 151785. https://doi.org/10.1016/j.cej.2024.151785
24. Li, G., An, T., Chen, J., Sheng, G., Fu, J., Chen, F., Zhang, S., Zhao, H. (2006). Photoelectrocatalytic decontamination of oilfield produced wastewater containing refractory organic pollutants in the presence of high concentration of chloride ions. *Journal of Hazardous Materials*, *138*(2), 392–400. https://doi.org/10.1016/j.jhazmat.2006.05.083
25. Liu, H., Lu, H., Hu, H. (2024). CO_2 capture and mineral storage: State of the art and future challenges. *Renewable and Sustainable Energy Reviews*, *189*, 113908. https://doi.org/10.1016/j.rser.2023.113908
26. Liu, J., Meng, F., Zhao, H., Xu, Y., Wang, K., Shi, C., Chen, Z. (2024). Optimization of CO_2 EOR and geological sequestration in high-water cut oil reservoirs. *Journal of Petroleum Exploration and Production Technology*, *14*(6), 1491–1504. https://doi.org/10.1007/s13202-024-01763-1
27. Mahdi, T. A., Aqrawi, A. A. M. (2014). Sequence stratigraphic analysis of the mid-cretaceous mishrif formation, southern Mesopotamian basin, IRAQ. *Journal of Petroleum Geology*, *37*(3), 287–312. https://doi.org/10.1111/jpg.12584
28. Mahlknecht, J., Steinich, B., Navarro de Leon, I. (2004). Groundwater chemistry and mass transfers in the Independence aquifer, central Mexico, by using multivariate statistics and mass-balance models. *Environmental Geology*, *45*(6), 781–795. https://doi.org/10.1007/s00254-003-0938-3
29. Matter, J. M., Broecker, W. S., Gislason, S. R., Gunnlaugsson, E., Oelkers, E. H., Stute, M., Sigurdardóttir, H., Stefansson, A., Alfreðsson, H. A., Aradóttir, E. S., Axelsson, G., Sigfússon, B., Wolff-Boenisch, D. (2011). The CarbFix Pilot Project–Storing carbon dioxide in basalt. *Energy Procedia*, *4*, 5579–5585. https://doi.org/10.1016/j.egypro.2011.02.546
30. Matter, M., Stute, M., Snæbjörnsdottir, S. Ó., Oelkers, E. H., Gislason, S. R., Aradottir, E. S., Sigfusson, B., Gunnarsson, I., Sigurdardottir, H., Gunnlaugsson, E., Axelsson, G., Alfredsson, H. A., Wolff-Boenisch, D., Mesfin, K., Taya, D. F. de la R., Hall, J., Dideriksen, K., Broecker, W. S. (2016). Rapid carbon mineralization for permanent disposal of anthropogenic carbon dioxide emissions. *Science*, *352*(6291), 1312–1314. https://doi.org/10.1126/science.aad8132
31. Mouedhen, I., Kemache, N., Pasquier, L.-C., Cecchi, E., Blais, J.-F., Mercier, G. (2017). Effect of pCO_2 on direct flue gas mineral carbonation at pilot scale. *Journal of Environmental Management*, *198*, 1–8. https://doi.org/10.1016/j.jenvman.2017.04.048
32. Nadeau, K., Mester, Z., Yang, L. (2018). The direct and accurate determination of major elements Ca, K, Mg and Na in water by HR-ICPMS. *Scientific Reports*, *8*(1), 17750. https://doi.org/10.1038/s41598-018-34028-z
33. Nowrouzi, I., Manshad, A. K., Mohammadi, A. H. (2019). Effects of dissolved carbon dioxide and ions in water on the dynamic interfacial tension of water and oil in the process of carbonated smart water injection into oil reservoirs. *Fuel*, *243*, 569–578. https://doi.org/10.1016/j.fuel.2019.01.069

34. Rodrigues, J. M., Fervari, M., Luoni, F., Monte, A. A., Miraglia, S., Banoori, S. (2016, November 7). Seismic Reservoir Characterization of Carbonate Reservoirs The Case Study of Mishrif Formation Zubair Field, Iraq. *Abu Dhabi International Petroleum Exhibition & Conference*. https://doi.org/10.2118/183289-MS
35. Sakai, T., McCurdy, E. (2022). ICP-MS Configuration and Optimization for Successful Routine Analysis of Undiluted Seawater. *Spectroscopy*, *37*(S9), 16–22. https://doi.org/10.56530/spectroscopy.ph3377i7
36. Satya Chanakya, I. V., Misra, S. (2024). Determination of trace elemental composition of $CaCO_3$: Application to mass limited abiogenic and biogenic carbonates. *Geochemistry, Geophysics, Geosystems*, *25*(2). https://doi.org/10.1029/2023GC011202
37. Søndergaard, J., Asmund, G., Larsen, M. M. (2015). Trace elements determination in seawater by ICP-MS with on-line pre-concentration on a Chelex-100 column using a 'standard' instrument setup. *MethodsX*, *2*, 323–330. https://doi.org/10.1016/j.mex.2015.06.003
38. Szymczycha-Madeja, A., Welna, M., Zabłocka-Malicka, M., Pohl, P., Szczepaniak, W. (2021). Development and validation of an analytical method for determination of Al, Ca, Cd, Fe, Mg and P in calcium-rich materials by ICP OES. *Molecules*, *26*(20), 6269. https://doi.org/10.3390/molecules26206269
39. Vásquez, L., Iriarte, A., Almeida, M., Villalobos, P. (2015). Evaluation of greenhouse gas emissions and proposals for their reduction at a university campus in Chile. *Journal of Cleaner Production*, *108*, 924–930. https://doi.org/10.1016/j.jclepro.2015.06.073
40. Werner, M., Hariharan, S. B., Bortolan, A. V., Zingaretti, D., Baciocchi, R., Mazzotti, M. (2013). Carbonation of activated serpentine for direct flue gas mineralization. *Energy Procedia*, *37*, 5929–5937. https://doi.org/10.1016/J.EGYPRO.2013.06.519
41. Wiebe, R., Gaddy, V. L. (2002). The solubility of carbon dioxide in water at various temperatures from 12 to 40° and at pressures to 500 atmospheres. critical phenomena. *Journal of the American Chemical Society*, *62*(4), 815–817. https://doi.org/10.1021/ja01861a033
42. Xue, K., Zhan, G., Wu, X., Zhang, H., Chen, Z., Chen, H., Li, J. (2023). Integration of membrane contactors and catalytic solvent regeneration for efficient carbon dioxide capture. *Journal of Membrane Science*, *684*, 121870. https://doi.org/10.1016/j.memsci.2023.121870
43. Zhu, B., Wilson, S., Zeyen, N., Raudsepp, M. J., Zolfaghari, A., Wang, B., Rostron, B. J., Snihur, K. N., von Gunten, K., Harrison, A. L., Alessi, D. S. (2022). Unlocking the potential of hydraulic fracturing flowback and produced water for CO_2 removal via mineral carbonation. *Applied Geochemistry*, *142*. https://doi.org/10.1016/j.apgeochem.2022.105345